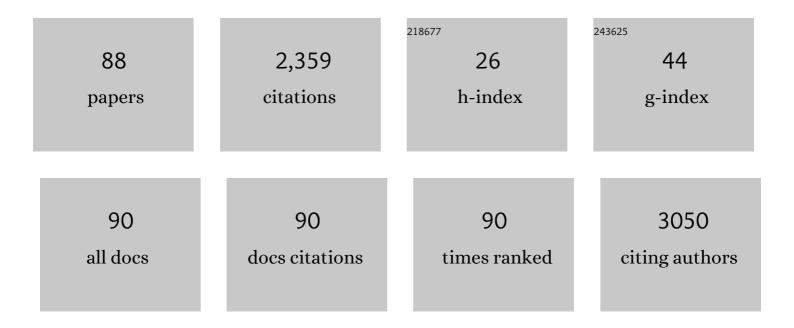
List of Publications by Year in descending order

Source: https://exaly.com/author-pdf/1560687/publications.pdf Version: 2024-02-01



ΤΗΓΟ ΥΛΝΙ ΜΛΙ SUM

#	Article	IF	CITATIONS
1	Standardized evaluation methodology and reference database for evaluating coronary artery centerline extraction algorithms. Medical Image Analysis, 2009, 13, 701-714.	11.6	295
2	Standardized evaluation methodology for 2-D-3-D registration. IEEE Transactions on Medical Imaging, 2005, 24, 1177-1189.	8.9	180
3	3D fusion of intravascular ultrasound and coronary computed tomography for in-vivo wall shear stress analysis: a feasibility study. International Journal of Cardiovascular Imaging, 2010, 26, 781-796.	1.5	69
4	Automatic segmentation, detection and quantification of coronary artery stenoses on CTA. International Journal of Cardiovascular Imaging, 2013, 29, 1847-1859.	1.5	69
5	Vessel Specific Coronary Artery Calcium Scoring. Academic Radiology, 2013, 20, 1-9.	2.5	67
6	An evaluation of automatic coronary artery calcium scoring methods with cardiac CT using the orCaScore framework. Medical Physics, 2016, 43, 2361-2373.	3.0	63
7	Vessel diameter measurements in gadolinium contrast-enhanced three-dimensional MRA of peripheral arteries. Magnetic Resonance Imaging, 2000, 18, 13-22.	1.8	56
8	Three-dimensional guide-wire reconstruction from biplane image sequences for integrated display in 3-d vasculature. IEEE Transactions on Medical Imaging, 2003, 22, 1252-1258.	8.9	55
9	Reproducibility, Accuracy, and Predictors of Accuracy for the Detection of Coronary Atherosclerotic Plaque Composition by Computed Tomography. Investigative Radiology, 2010, 45, 693-701.	6.2	53
10	Robust Shape Regression for Supervised Vessel Segmentation and its Application to Coronary Segmentation in CTA. IEEE Transactions on Medical Imaging, 2011, 30, 1974-1986.	8.9	51
11	Epicardial fat volume is related to atherosclerotic calcification in multiple vessel beds. European Heart Journal Cardiovascular Imaging, 2015, 16, 1264-1269.	1.2	50
12	The Reduction of Endplate Fractures During Balloon Vertebroplasty. Spine, 2005, 30, 1840-1845.	2.0	47
13	Semiautomatic carotid lumen segmentation for quantification of lumen geometry in multispectral MRI. Medical Image Analysis, 2012, 16, 1202-1215.	11.6	47
14	Ultrasound Aided Vertebral Level Localization for Lumbar Surgery. IEEE Transactions on Medical Imaging, 2017, 36, 2138-2147.	8.9	47
15	Accurate 3D temperature dosimetry during hyperthermia therapy by combining invasive measurements and patient-specific simulations. International Journal of Hyperthermia, 2015, 31, 686-692.	2.5	45
16	Evaluation of 2D and 3D ultrasound tracking algorithms and impact on ultrasoundâ€guided liver radiotherapy margins. Medical Physics, 2018, 45, 4986-5003.	3.0	43
17	CT-based patient modeling for head and neck hyperthermia treatment planning: Manual versus automatic normal-tissue-segmentation. Radiotherapy and Oncology, 2014, 111, 158-163.	0.6	41
18	Guide wire reconstruction and visualization in 3DRA using monoplane fluoroscopic imaging. IEEE Transactions on Medical Imaging, 2005, 24, 612-623.	8.9	38

#	Article	IF	CITATIONS
19	Epicardial Fat Volume and the Risk of AtrialÂFibrillation in the General Population Free of Cardiovascular Disease. JACC: Cardiovascular Imaging, 2017, 10, 1405-1407.	5.3	38
20	Automatic needle detection and real-time Bi-planar needle visualization during 3D ultrasound scanning of the liver. Medical Image Analysis, 2019, 53, 104-110.	11.6	37
21	Fast and robust 3D ultrasound registration – Block and game theoretic matching. Medical Image Analysis, 2015, 20, 173-183.	11.6	30
22	Microvascular damage assessed by optical coherence tomography angiography for glaucoma diagnosis: a systematic review of the most discriminative regions. Acta Ophthalmologica, 2020, 98, 537-558.	1.1	30
23	Bone Displacement and the Role of Longitudinal Ligaments During Balloon Vertebroplasty in Traumatic Thoracolumbar Fractures. Spine, 2005, 30, 1832-1839.	2.0	29
24	Accuracy evaluation of direct navigation with an isocentric 3D rotational X-ray system. Medical Image Analysis, 2006, 10, 113-124.	11.6	28
25	Three-dimensional registration of histology of human atherosclerotic carotid plaques to in-vivo imaging. Journal of Biomechanics, 2010, 43, 2087-2092.	2.1	28
26	Small coronary calcifications are not detectable by 64-slice contrast enhanced computed tomography. International Journal of Cardiovascular Imaging, 2011, 27, 143-152.	1.5	27
27	The use of atlas registration and graph cuts for prostate segmentation in magnetic resonance images. Medical Physics, 2015, 42, 1614-1624.	3.0	27
28	Needle Tip Visibility in 3D Ultrasound Images. CardioVascular and Interventional Radiology, 2018, 41, 145-152.	2.0	26
29	Dynamic coronary roadmapping via catheter tip tracking in X-ray fluoroscopy with deep learning based Bayesian filtering. Medical Image Analysis, 2020, 61, 101634.	11.6	26
30	Automatic Collateral Scoring From 3D CTA Images. IEEE Transactions on Medical Imaging, 2020, 39, 2190-2200.	8.9	26
31	Three-Dimensional Rotational X-Ray Navigation for Needle Guidance in Percutaneous Vertebroplasty: An Accuracy Study. Spine, 2006, 31, 1359-1364.	2.0	25
32	Image-guided vascular neurosurgery based on three-dimensional rotational angiography. Journal of Neurosurgery, 2007, 106, 501-506.	1.6	25
33	Temperature simulations in hyperthermia treatment planning of the head and neck region. Strahlentherapie Und Onkologie, 2014, 190, 1117-1124.	2.0	25
34	An automatic registration method for pre―and postâ€interventional CT images for assessing treatment success in liver RFA treatment. Medical Physics, 2015, 42, 5559-5567.	3.0	24
35	Non-Rigid Registration of Liver CT Images for CT-Guided Ablation of Liver Tumors. PLoS ONE, 2016, 11, e0161600.	2.5	24
36	Automatic online layer separation for vessel enhancement in X-ray angiograms for percutaneous coronary interventions. Medical Image Analysis, 2017, 39, 145-161.	11.6	23

#	Article	IF	CITATIONS
37	Three-Dimensional Rotational X-ray Imaging for Spine Surgery. Spine, 2005, 30, 556-561.	2.0	22
38	The relevance of MRI for patient modeling in head and neck hyperthermia treatment planning: A comparison of CT and CTâ€MRI based tissue segmentation on simulated temperature. Medical Physics, 2014, 41, 123302.	3.0	22
39	Regression-Based Cardiac Motion Prediction From Single-Phase CTA. IEEE Transactions on Medical Imaging, 2012, 31, 1311-1325.	8.9	21
40	Automated versus manual segmentation of atherosclerotic carotid plaque volume and components in CTA: associations with cardiovascular risk factors. International Journal of Cardiovascular Imaging, 2012, 28, 877-887.	1.5	21
41	Contour segmentation of the intima, media, and adventitia layers in intracoronary OCT images: application to fully automatic detection of healthy wall regions. International Journal of Computer Assisted Radiology and Surgery, 2017, 12, 1923-1936.	2.8	21
42	Selective Visualization of Vector Fields. Computer Graphics Forum, 1994, 13, 339-347.	3.0	19
43	Review on Retrospective Procedures to Correct Retinal Motion Artefacts in OCT Imaging. Applied Sciences (Switzerland), 2019, 9, 2700.	2.5	19
44	Noninvasive Magnetic Resonance to Three-Dimensional Rotational X-Ray Registration of Vertebral Bodies for Image-Guided Spine Surgery. Spine, 2004, 29, 293-297.	2.0	18
45	Additional Diagnostic Value of Integrated Analysis of Cardiac CTA and SPECT MPI Using the SMARTVis System in Patients with Suspected Coronary Artery Disease. Journal of Nuclear Medicine, 2014, 55, 50-57.	5.0	18
46	MRI integration into treatment planning of head and neck tumors: Can patient immobilization be avoided?. Radiotherapy and Oncology, 2015, 115, 191-194.	0.6	18
47	Registration of <formula formulatype="inline"><tex notation="TeX">\$3{m D}+{m t}\$</tex></formula> Coronary CTA and Monoplane <formula formulatype="inline"><tex Notation="TeX"&gt;\$2{m D}+{m t}\$</tex </formula> X-Ray Angiography. IEEE Transactions on Medical Imaging, 2013, 32, 919-931.	8.9	17
48	Random Forest-Based Bone Segmentation in Ultrasound. Ultrasound in Medicine and Biology, 2017, 43, 2426-2437.	1.5	17
49	autoTICI: Automatic Brain Tissue Reperfusion Scoring on 2D DSA Images of Acute Ischemic Stroke Patients. IEEE Transactions on Medical Imaging, 2021, 40, 2380-2391.	8.9	17
50	Calcification Locates to Transglutaminases in Advanced Human Atherosclerotic Lesions. American Journal of Pathology, 2009, 175, 1374-1379.	3.8	16
51	OCTA Multilayer and Multisector Peripapillary Microvascular Modeling for Diagnosing and Staging of Glaucoma. Translational Vision Science and Technology, 2020, 9, 58.	2.2	16
52	Adaptive optics ophthalmoscopy: a systematic review of vascular biomarkers. Survey of Ophthalmology, 2022, 67, 369-387.	4.0	15
53	Feasibility and relevance of discrete vasculature modeling in routine hyperthermia treatment planning. International Journal of Hyperthermia, 2019, 36, 800-810.	2.5	14
54	Global, geometric, and feature-based techniques for vector field visualization. Future Generation Computer Systems, 1999, 15, 87-98.	7.5	13

#	Article	IF	CITATIONS
55	Navigation with Three-dimensional Rotational Radiographic Data for Transpedicular Percutaneous Needle Introduction: Feasibility and Comparison with Fluoroscopic Guidance. Journal of Vascular and Interventional Radiology, 2006, 17, 1511-1518.	0.5	13
56	Semiautomated registration of pre- and intraoperative CT for image-guided percutaneous liver tumor ablation interventions. Medical Physics, 2017, 44, 3718-3725.	3.0	13
57	Validation of automated Alberta Stroke Program Early CT Score (ASPECTS) software for detection of early ischemic changes on non-contrast brain CT scans. Neuroradiology, 2021, 63, 491-498.	2.2	11
58	4D Ultrasound Tracking of Liver and its Verification for TIPS Guidance. IEEE Transactions on Medical Imaging, 2016, 35, 52-62.	8.9	10
59	Multiple-correlation similarity for block-matching based fast CT to ultrasound registration in liver interventions. Medical Image Analysis, 2019, 53, 132-141.	11.6	10
60	An Evaluation of CNN-based Liver Segmentation Methods using Multi-types of CT Abdominal Images from Multiple Medical Centers. , 2019, , .		9
61	Spatio-temporal deep learning for automatic detection of intracranial vessel perforation in digital subtraction angiography during endovascular thrombectomy. Medical Image Analysis, 2022, 77, 102377.	11.6	9
62	Augmented reality navigation for minimally invasive craniosynostosis surgery: a phantom study. International Journal of Computer Assisted Radiology and Surgery, 2022, 17, 1453-1460.	2.8	9
63	Multimodal markers for technology-independent integration of augmented reality devices and surgical navigation systems. Virtual Reality, 2022, 26, 1637-1650.	6.1	9
64	3D/3D registration of coronary CTA and biplane XA reconstructions for improved image guidance. Medical Physics, 2014, 41, 091909.	3.0	8
65	PCA-derived respiratory motion surrogates from X-ray angiograms for percutaneous coronary interventions. International Journal of Computer Assisted Radiology and Surgery, 2015, 10, 695-705.	2.8	8
66	Inter-rater reliability for assessing intracranial collaterals in patients with acute ischemic stroke: comparing 29 raters and an artificial intelligence-based software. Neuroradiology, 2022, 64, 2277-2284.	2.2	8
67	Endpoint localization in guide wire tracking during endovascular interventions1. Academic Radiology, 2003, 10, 1424-1432.	2.5	7
68	Carotid artery segmentation and plaque quantification in CTA. , 2009, , .		7
69	Improved Segmentation of Multiple Cavities of the Heart in Wide-View 3-D Transesophageal Echocardiograms. Ultrasound in Medicine and Biology, 2015, 41, 1991-2000.	1.5	7
70	Semi-automatic MRI segmentation and volume quantification of intra-plaque hemorrhage. International Journal of Computer Assisted Radiology and Surgery, 2015, 10, 67-74.	2.8	7
71	Signal-carrying speckle in optical coherence tomography: a methodological review on biomedical applications. Journal of Biomedical Optics, 2022, 27, .	2.6	7
72	Multi-modal and multi-scale clinical retinal imaging system with pupil and retinal tracking. Scientific Reports, 2022, 12, .	3.3	7

#	Article	IF	CITATIONS
73	Fusion of fibrous cap thickness and wall shear stress to assess plaque vulnerability in coronary arteries: a pilot study. International Journal of Computer Assisted Radiology and Surgery, 2016, 11, 1779-1790.	2.8	6
74	Optical Coherence Tomography Imaging of the Lamina Cribrosa: Structural Biomarkers in Nonglaucomatous Diseases. Journal of Ophthalmology, 2021, 2021, 1-31.	1.3	6
75	Virtual extensions improve perception-based instrument alignment using optical see-through devices. IEEE Transactions on Visualization and Computer Graphics, 2021, 27, 4332-4341.	4.4	6
76	Averaging Centerlines: Mean Shift on Paths. Lecture Notes in Computer Science, 2008, 11, 900-907.	1.3	6
77	Classification of hemodynamically significant stenoses from dynamic CT perfusion and CTA myocardial territories. Medical Physics, 2017, 44, 1347-1358.	3.0	4
78	Mesenteric artery calcium scoring: a potential screening method for chronic mesenteric ischemia. European Radiology, 2021, 31, 4212-4220.	4.5	4
79	Automatic Segmentation of the Optic Nerve Head Region in Optical Coherence Tomography: A Methodological Review. Computer Methods and Programs in Biomedicine, 2022, 220, 106801.	4.7	4
80	Accuracy of semi-automated versus manual localisation of liver tumours in CT-guided ablation procedures. European Radiology, 2018, 28, 4978-4984.	4.5	3
81	Cortical and vascular probability maps for analysis of human brain in computed tomography images. , 2017, , .		2
82	3D Catheter Tip Tracking in 2D X-Ray Image Sequences Using a Hidden Markov Model and 3D Rotational Angiography. Lecture Notes in Computer Science, 2015, , 38-49.	1.3	2
83	Blockâ€matchingâ€based registration to evaluate ultrasound visibility of percutaneous needles in liverâ€mimicking phantoms. Medical Physics, 2021, 48, 7602.	3.0	2
84	Automatic artery/vein classification in 2D-DSA images of stroke patients. , 2022, , .		2
85	Quantitative Analysis of Geometry and Lateral Symmetry of Proximal Middle Cerebral Artery. Journal of Stroke and Cerebrovascular Diseases, 2017, 26, 2427-2434.	1.6	1
86	Automated Quantification of Bileaflet Mechanical Heart Valve Leaflet Angles in CT Images. IEEE Transactions on Medical Imaging, 2019, 38, 753-761.	8.9	1
87	Efficiently compressing 3D medical images for teleinterventions via CNNs and anisotropic diffusion. Medical Physics, 2021, 48, 2877-2890.	3.0	1
88	Automatic scan range for dose-reduced multiphase CT imaging of the liver utilizing CNNs and Gaussian models. Medical Image Analysis, 2022, 78, 102422.	11.6	1